The Astrophysical Journal Letters, 896:L18 (9pp), 2020 June 20 https://doi.org/10.3847/2041-8213/ab96be


# Coronal-jet-producing Minifilament Eruptions as a Possible Source of Parker Solar Probe Switchbacks

Alphonse C. Sterling[1] and Ronald L. Moore[1,2]
[1] NASA/Marshall Space Flight Center, Huntsville, AL 35812, USA
[2] Center for Space Plasma and Aeronomic Research, University of Alabama in Huntsville, Huntsville, AL 35805, USA
*Received 2020 March 2; revised 2020 May 18; accepted 2020 May 20; published 2020 June 15*

## Abstract

The Parker Solar Probe (PSP) has observed copious rapid magnetic field direction changes in the near-Sun solar wind. These features have been called "switchbacks," and their origin is a mystery. But their widespread nature suggests that they may be generated by a frequently occurring process in the Sun's atmosphere. We examine the possibility that the switchbacks originate from coronal jets. Recent work suggests that many coronal jets result when photospheric magnetic flux cancels, and forms a small-scale "minifilament" flux rope that erupts and reconnects with coronal field. We argue that the reconnected erupting-minifilament flux rope can manifest as an outward propagating Alfvénic fluctuation that steepens into an increasingly compact disturbance as it moves through the solar wind. Using previous observed properties of coronal jets that connect to coronagraph-observed white-light jets (a.k.a. "narrow CMEs"), along with typical solar wind speed values, we expect the coronal-jet-produced disturbances to traverse near-perihelion PSP in $\lesssim$25 minutes, with a velocity of $\sim$400 km s$^{-1}$. To consider further the plausibility of this idea, we show that a previously studied series of equatorial latitude coronal jets, originating from the periphery of an active region, generate white-light jets in the outer corona (seen in STEREO/COR2 coronagraph images; 2.5–15 $R_{\odot}$), and into the inner heliosphere (seen in Solar-Terrestrial Relations Observatory (STEREO)/Hi1 heliospheric imager images; 15–84 $R_{\odot}$). Thus it is tenable that disturbances put onto open coronal magnetic field lines by coronal-jet-producing erupting-minifilament flux ropes can propagate out to PSP space and appear as switchbacks.

*Unified Astronomy Thesaurus concepts:* Solar filament eruptions (1981); Solar magnetic fields (1503); Solar magnetic reconnection (1504); Solar wind (1534)

*Supporting material:* animations

## 1. Introduction

The Parker Solar Probe (PSP) mission (Bale et al. 2016; Fox et al. 2016; Kasper et al. 2016) has for the first time carried out in situ observations in the near-Sun solar wind, reaching ~35 $R_{\odot}$ in 2018 November and also in 2019 April. An exciting early observation from the mission is that the near-Sun magnetic field is replete with transient, kinked structures that have been called "switchbacks" (Bale et al. 2019; Kasper et al. 2019; Dudok de Wit et al. 2020; Mozer et al. 2020). Similar structures were also seen earlier (e.g., Kahler et al. 1996; Yamauchi et al. 2004; Suess 2007). The source of these features is not understood. A possibility that we investigate here is that solar coronal jets might be responsible for the switchbacks (as suggested by, e.g., Horbury et al. 2020).

Here we examine the possibility that a recently suggested process for making coronal jets, based on the eruption of small-scale filaments and their enveloping field that reconnects with the coronal field, results in the switchbacks.

## 2. Coronal Jets and White-light Jets

### 2.1. Coronal Jets

Coronal jets have been observed for some time at X-ray (e.g., Shibata et al. 1992; Cirtain et al. 2007) and EUV (e.g., Nisticò et al. 2009) wavelengths. They are frequently occurring phenomena, with a rate of about 60 day$^{-1}$ in polar coronal holes alone (Savcheva et al. 2007). For reviews of jets, see Shibata & Magara (2011), Raouafi et al. (2016), and Hinode Review Team et al. (2019).

Recent observations support that at least many, if not most or all, coronal jets result from the eruption of a small-scale filament, or *minifilament*, and its enveloping magnetic field. Sterling et al. (2015) proposed a "minifilament-eruption model" for coronal jets, and argued that the entire coronal-jet event is a scaled-down version of the larger-scale eruptions that create typical solar flares and CMEs. Apparently almost all coronal jets, at least those in quiet Sun and coronal hole regions, are produced by such eruptions. Often the small-scale erupting field contains cool material (appearing as the minifilament) in the core of the erupting magnetic arcade (e.g., Moore et al. 2010; Shen et al. 2012, 2017, 2019; Hong et al. 2014; McGlasson et al. 2019), where the eruption can be either ejective or confined (Sterling et al. 2015). We cannot, however, totally rule out that some other process, such as the much-earlier-suggested emerging-flux mechanism (Shibata et al. 1992; Yokoyama & Shibata 1995), might produce some jets and expel cool material into the corona.

Other observations show that the coronal jets originate at photospheric locations where magnetic flux cancellation occurs under the pre-eruption minifilament (e.g., Shen et al. 2012; Hong et al. 2014; Young & Muglach 2014a, 2014b; Panesar et al. 2016b). We have found observational evidence that in many cases magnetic flux cancellation creates the minifilament flux rope and triggers the eruption of the flux rope and its enveloping magnetic arcade, and this eruption produces the coronal jet (Panesar et al. 2016b, 2017, 2018a; Sterling et al. 2017; McGlasson et al. 2019). An alternative view argued by Kumar et al. (2018) is that often shearing and/or rotational

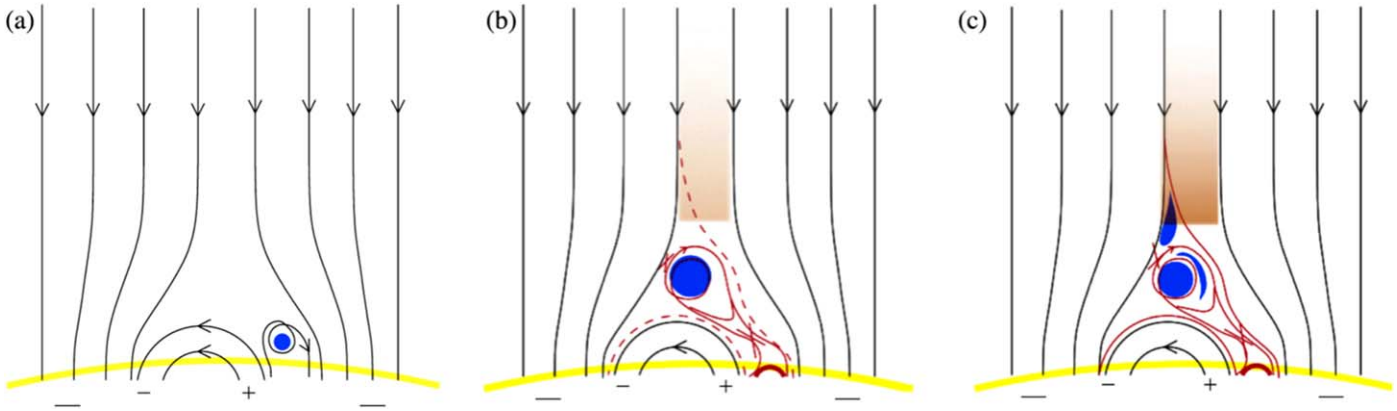


**Figure 1.** Schematic showing jet generation via a "minifilament eruption model," as proposed in Sterling et al. (2015). This version of the schematic appeared in Sterling et al. (2018), and includes an adjustment due to Moore et al. (2018). (a) Cross-sectional view of a 3D positive-polarity anemone-type field inside of a majority negative-polarity ambient field (which we assume to open into the heliosphere). One side of the anemone is highly sheared and contains a minifilament (blue circle). (b) Here the minifilament is erupting and undergoing reconnection in two locations: (1) *internal* ("tether-cutting" type) reconnection (larger red cross), with the solid red lines showing the resulting reconnected fields; the thick red semicircle represents the "jet bright point" (JBP) at the jet's base; and (2) *external* (a.k.a. "interchange" or "breakout" reconnection) occurs at the site of the smaller red cross, with the dashed lines indicating its two reconnection products. (c) If the external reconnection proceeds far enough, then the minifilament material can leak out onto the open field. Shaded areas represent heated jet material visible in X-rays and some SDO/AIA EUV channels as the jet's spire. See, e.g., Sterling et al. (2015) or Moore et al. (2018) for a more detailed description.

photospheric motion is responsible for the buildup of energy along the minifilament channel that gets released through eruption and produces the jet.

Figure 1 shows the basic minifilament-eruption jet-production idea of Sterling et al. (2015). Figure 1(a) shows a cross-sectional view of a 3D positive-polarity anemone-type field inside of a majority negative-polarity ambient open field. One side of the anemone is highly sheared (and often twisted) and contains a minifilament (blue circle). In Figure 1(b) the minifilament field is erupting and undergoing reconnection in two locations: (1) *internal* ("tether-cutting" type) reconnection (larger red cross), with the solid red lines showing the resulting reconnected fields, and where the thick red semicircle represents the "jet bright point" (JBP) at the jet's base; and (2) *external* (a.k.a. "interchange" or "breakout") reconnection occurs at the site of the smaller red cross, with the dashed lines indicating its two reconnection products. Figure 1(c) shows that if the external reconnection proceeds far enough, then the minifilament material can leak out onto the open field. Shaded areas represent heated jet material visible in X-rays and some Solar Dynamics Observatory (SDO)/Atmospheric Imaging Assembly (AIA) EUV channels as the jet's spire. This picture has been successfully simulated by Wyper et al. (2017, 2018; they refer to this "minifilament-eruption model for jets" as a "breakout model for jets," since breakout-type reconnection is integral to the jet's production).

Active region (AR) coronal jets similarly show evidence that they are made from small-scale eruptions, and that these eruptions are prepared and triggered by magnetic flux cancellation. It seems, however, as if the eruptions leading to AR jets less frequently (than in non-AR areas) carry cool material that appears as a minifilament, although evidence indicates that a minifilament-type flux-rope field still erupts to make the AR jets (Sterling et al. 2016, 2017).

### 2.2. White-light Jets and Twists on Coronal Jets

Coronal jets are capable of producing features observed in coronagraphs called "narrow CMEs" or "white-light jets" (e.g., Wang et al. 1998; Nisticò et al. 2009; Moore et al. 2015; Sterling et al. 2016). Such studies showed a clear connection between coronal jets on the Sun and the white-light jets observed with either the Solar-Terrestrial Relations Observatory (STEREO) COR1 coronagraph (Nisticò et al. 2009, 2010; Paraschiv et al. 2010), or the LASCO C2 coronagraph (Wang et al. 1998; Moore et al. 2015; Sterling et al. 2016). In other cases, jets can apparently propel outward—or at least accompany—broader "bubble-like" CMEs (e.g., Bemporad et al. 2005; Shen et al. 2012; Alzate & Morgan 2016; Panesar et al. 2016a; Miao et al. 2018; Duan et al. 2019; Solanki et al. 2019); our focus here, however, is on the narrow CMEs.

Several studies have found twist on jets (e.g., Pike & Mason 1998). A few such investigations have measured the number of turns a jet undergoes over its lifetime; Shen et al. (2011b) found a jet to undergo 1.2–2.6 turns, while Chen et al. (2012) estimated the same jet to undergo 3.6 turns. Hong et al. (2013) estimated a different jet, one that may have produced a white-light jet, to undergo 0.9 turns. Moore et al. (2013) found that 24 of 29 (83%) random polar jets that they examined had one-half or fewer turns, while the remaining five events had up to 2.5 turns. Liu et al. (2019) studied 30 off-limb "large-scale rotational" coronal jets, and found that they all underwent at least 1.3 turns and 80% of them rotated less than 2.8 turns, with the one with maximal rotation having 4.7 turns. References in Liu et al. (2019) discuss other papers with jet-twist measurements.

Moore et al. (2015) studied 14 jets that produced white-light jets, and found that they had twist values of one-half to 2.5 turns. They argued that an erupting twisted flux rope (which in subsequent papers we argue is a minifilament flux rope) can inject twist onto the white-light jet. A conclusion of their study was that all of the coronal jets that made white-light jets in their study had a comparatively large amount of twist in the spire of the coronal jets when observed in AIA 304 Å. Thus it was apparent that the twist was an important factor for the coronal jets to make it out to a few $R_\odot$ into the corona.

Figure 2 shows our picture for how a coronal-jet-producing minifilament eruption could launch a white-light jet. Initially the minifilament field that erupts to form the coronal jet would carry twist, as in Figure 2(a). When this twisted erupting flux rope strikes ambient field of opposite polarity in Figure 2(b)

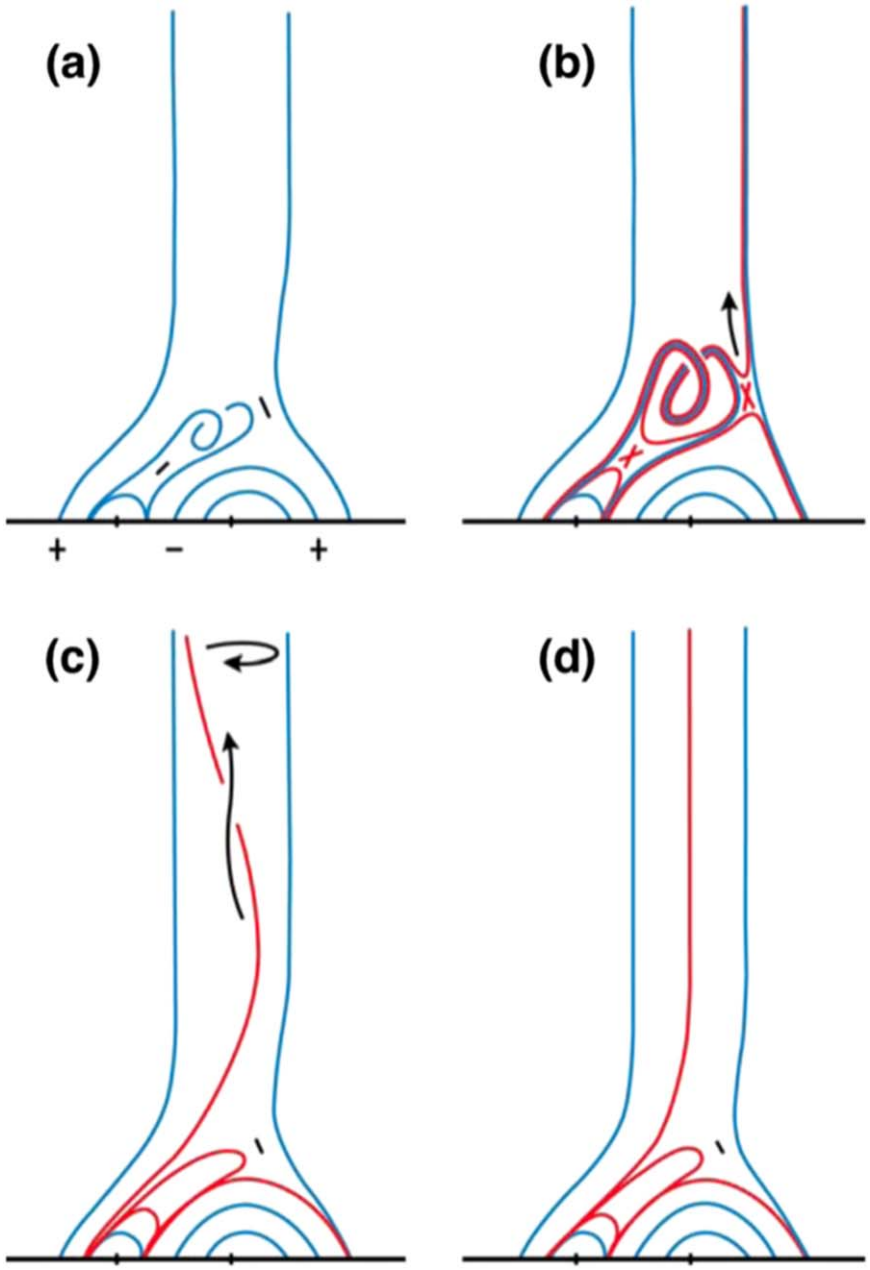


**Figure 2.** Schematic from Moore et al. (2015) of the generation of the magnetic-untwisting wave in an ejective minifilament-eruption (blowout) jet by the blowout and interchange reconnection of initially closed magnetic field at the base of the jet. At the time of original publication in Moore et al. (2015), the full minifilament eruption model (Figure 1) was still being developed, but several critical components of that model are already included here. Panels (a) and (b) show what we now call the minifilament field erupting, basically following Figure 1. In this case, however, the schematic emphasizes that the erupting-minifilament field contains twist. That twist is imparted to the ambient open field via the external reconnection in (b). This results in a relaxation (untwisting) of the reconnected twisted ambient coronal field in (c). Eventually the near-original setup ensues (d), but with the original twist in the minifilament field now removed from in and near the jet's base field. In this representation, the erupting-minifilament field has right-handed twist; this is imparted to the spire field, which then spins in a clockwise direction (viewed from above) to undo the imparted right-handed twist.

(corresponding to Figure 1(b)) and undergoes external reconnection, that reconnection transfers twist onto the ambient open field, as proposed by Shibata & Uchida (1986). This twist would propagate outward (Figure 2(c)) as an Alfvénic twist-wave packet, driving the white-light jet seen in coronagraph images. Eventually (Figure 2(d)) the near-original setup is recovered, but with the imparted twist from the reconnected minifilament field now removed from in and near the jet's base field.

## 3. Possible Production of Switchbacks by Propagating Magnetic Twist on White-light Jets

Figure 3 is a continuation of Figure 2, showing how the twist imparted to an open field by a coronal-jet-producing minifilament eruption evolves into a switchback, where the yellow circles represent the Sun, and the blue lines represent heliospheric field lines that are curved, following a Parker spiral, with respect to a radial line (black). The twist put onto the white-light jet (Figure 2(c)) will continue to propagate out into the heliosphere. In Figure 3(a), the twist is shown as an

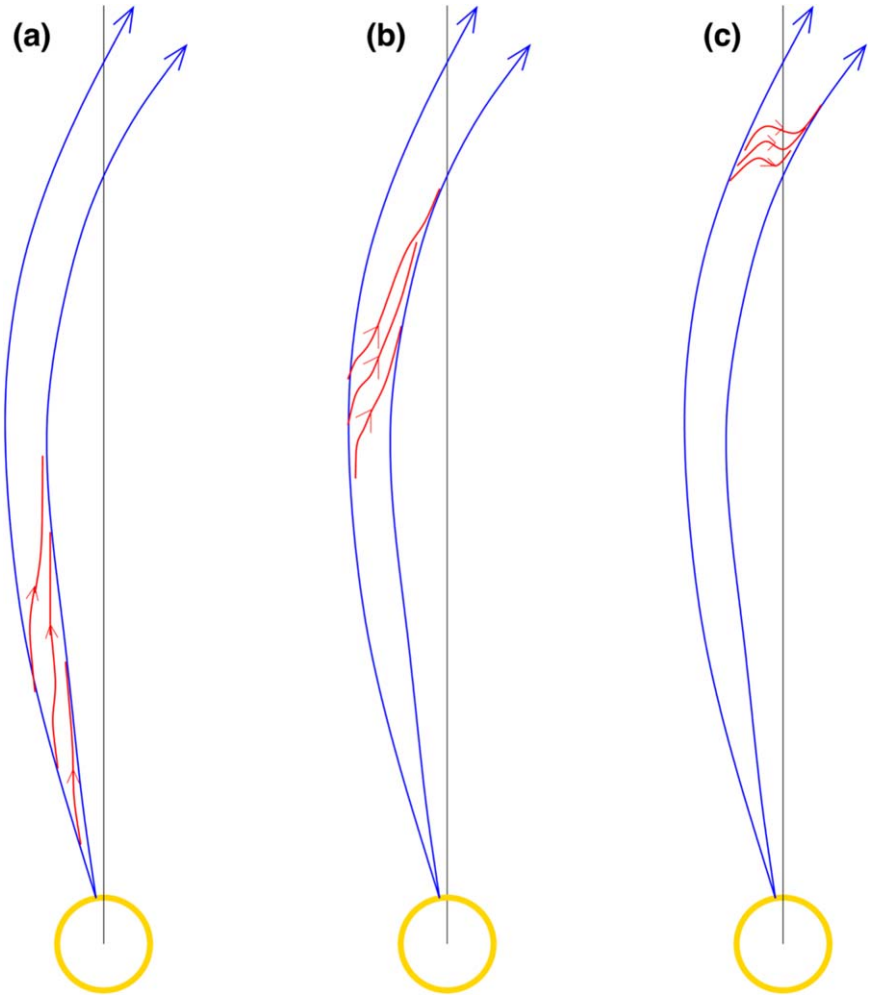


**Figure 3.** Schematic showing a continuation of Figure 2, where the twist imparted to the ambient coronal field in Figure 2(c) continues to propagate outward. Here, the yellow circles represent the Sun, and the blue lines represent heliospheric field lines that are curved with respect to a radial line (black), following a Parker spiral. In (a), the wave imparted to the coronal field in Figure 2(c) becomes the red disturbance that appears as a low-pitch twist-wave packet moving outward (the radial extent of the twist packet would be comparable to a solar radius, and so its extent is exaggerated by a factor of a few times compared to the Sun in this schematic representation). Panel (b) shows how the pitch of the disturbance is expected to increase as it moves further from the Sun, into a regime with lower Alfvén speed compared to that in the corona, as described in the text. In (c), this pitch-angle steepening of the disturbance continues as it moves even further from the Sun, perhaps appearing as a switchback by the time it encounters PSP.

extension to the situation in Figure 2(c), with the twist having about the same small pitch angle as seen in the C2 images of Figure 6 of Moore et al. (2015).

In Figure 3(a), the twist imparted to the ambient coronal field in Figure 2(c) continues to propagate outward, becoming the red disturbance that appears as a low-pitch twist-wave packet moving outward (the radial extent of the twist packet would be comparable to a solar radius, and so is exaggerated by a factor of ∼5 compared to the Sun in this schematic representation). Figure 3(b) shows the pitch of the disturbance increasing as it moves farther from the Sun. This is our expectation, because it moves into a regime with progressively lower Alfvén velocity. (In the corona, the Alfvén velocity, $V_A \approx 1000$ km s$^{-1}$. At the first PSP perihelion, Bale et al. 2019 report $V_A \sim 100$ km s$^{-1}$ in the solar wind at 36.6 $R_\odot$.) Based on Moore et al. (2015), the disturbance in C2 has length $L$ comparable to $R_\odot$. The front of the disturbance moves more slowly than its rear, resulting in a "compression" (increasing pitch angle) of the disturbance. In Figure 3(c), this pitch-angle steepening of the disturbance continues as it moves even farther from the Sun, appearing as a switchback by the time it encounters PSP.

PSP would detect the Alfvén-wave packet as the packet flows and propagates by. The radial speed of the packet will vary depending on its distance from the Sun. At the time of its launch in the low corona, the packet would have a speed of about that of the local coronal Alfvén speed (∼1000 km s$^{-1}$), with a solar wind velocity, $V_{SW}$, of practically zero. At PSP, the Alfvén velocity will be ∼100 km s$^{-1}$ as mentioned above, but it will be riding in the solar wind with $V_{SW} \approx 300$ km s$^{-1}$ (which is the baseline solar-wind speed reported by Kasper et al. 2019 during the first PSP perihelion passage); that is, it will pass PSP at about 400 km s$^{-1}$.

The length of the packet, $L$, at the Sun will be about $V_A \times \tau$, where we can take $\tau \approx 600$ s, since a typical coronal jet lasts about 10 minutes (e.g., Savcheva et al. 2007). So the pulse's length near the Sun, $L_{cor}$, would be $L_{cor} \sim 600{,}000$ km. At PSP, a packet of this length traveling at 400 km s$^{-1}$ would appear as a pulse passing the spacecraft in 1500 s, i.e., ∼25 minutes. The Alfvén-wave packet's length at the spacecraft, $L_{PSP}$, however, will be reduced from what it was in the corona, via the above-argued pitch-angle-steepening rationale. Thus the passage of the pulse (the switchback) past PSP should

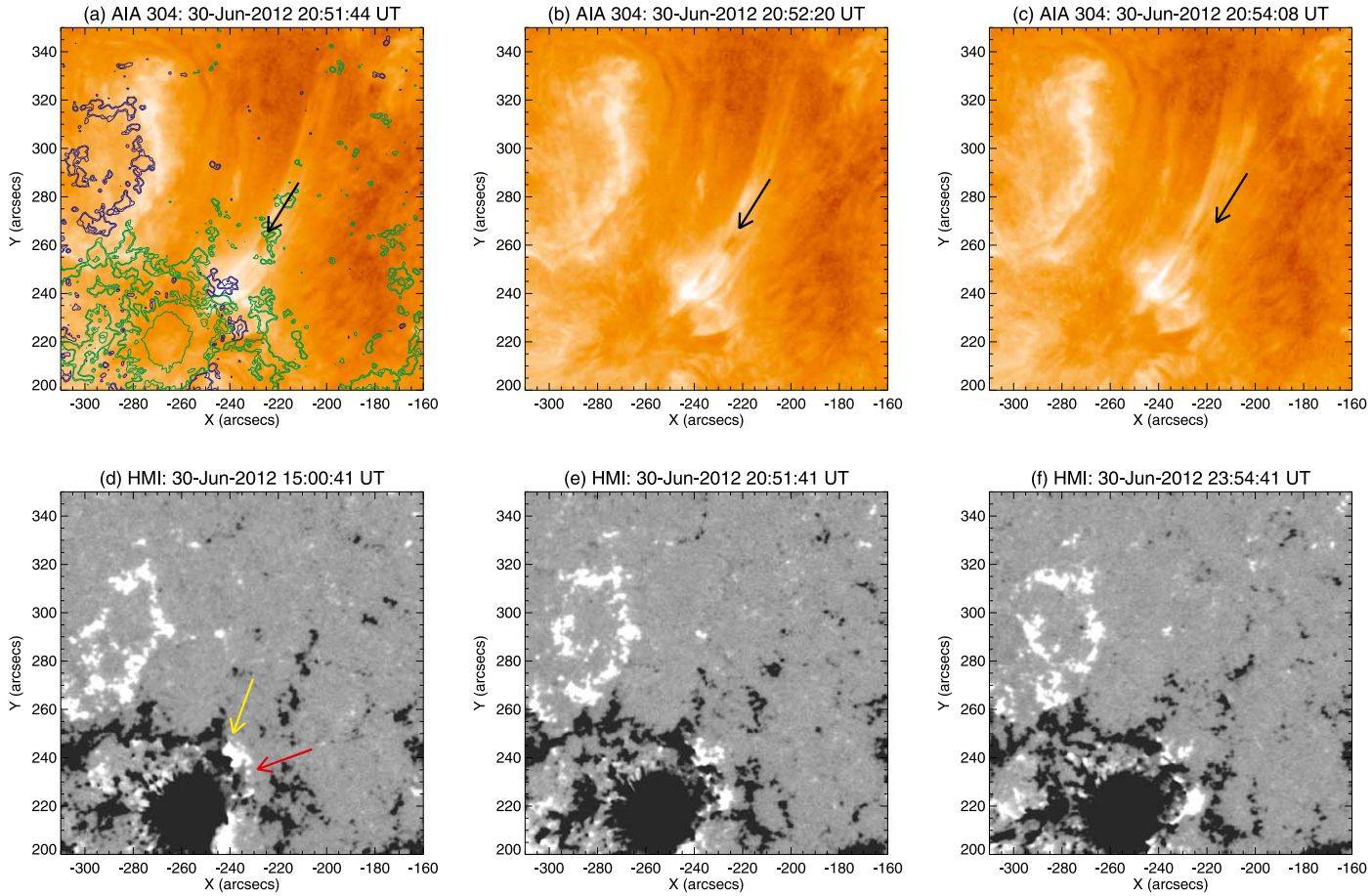


**Figure 4.** Coronal jets from NOAA AR 11513 (studied in detail in Sterling et al. 2016). Panels (a)–(c) show SDO/AIA 304 Å subframes, showing jet J5 of Table 1. Arrows show absorbing erupting-filament material undergoing spinning motion in the successive frames. Panel (a) is overlaid with the magnetogram of (e), where blue and green contours, respectively, outline positive and negative polarities. Panels (d)–(f) show SDO/HMI magnetograms of the region, with white and black, respectively, representing positive and negative polarities. Arrows in (d) show two neutral lines that are the source locations of the jets in Table 1; the positive-polarity patch between the arrows decreases with time due to flux cancellation. According to the model in Figure 1, this flux cancellation builds the minifilament flux ropes that erupt to drive the jets, as in (a)–(c). An animation of this figure is available with the top portion corresponding to panels (a)–(c). It begins on 2012 June 30 at 19:00:44 UT and ends the same day at 23:50:32 UT. Its realtime duration is 48 s. The bottom part of the animation shows the panel (d)–(f) sequence. It also begins on 2012 June 30 but runs from 15:00:41 to 23:57:41 UT. The realtime duration is only 18 s.

(An animation of this figure is available.)

be less than about 25 minutes. Smaller-scale "network jets" (or "jetlets"; e.g., Raouafi & Stenborg 2014) appear to work like typical coronal jets (Panesar et al. 2018b). Thus these smaller events plausibly produce many briefer switchbacks in the solar wind. Observed switchbacks have durations ranging from less than 1 s to more than 1 hour (e.g., Dudok de Wit et al. 2020).

## 4. Observations of Coronal Jets in the STEREO Outer Corona

While Sections 2 and 3 present a scenario whereby coronal jets might theoretically make PSP switchbacks, there still remains the question of whether coronal-jet effects can actually propagate out to the distances of tens of solar radii where they might be detected by PSP. As pointed out in Section 1, there have been several observations of the effects of coronal jets out to the STEREO/COR1 (1.5–4 $R_{\odot}$; Howard et al. 2008) and LASCO C2 (1.5–6 $R_{\odot}$) distances. Polar coronal jets have been tracked even farther, into the STEREO/COR2 (2.5–15 $R_{\odot}$) field of view (FOV), and then as density enhancements at substantial fractions of an au in 3D reconstructions from Solar Mass Ejection Imager (SMEI) data in recent studies (Yu et al. 2014, 2016).

In this section we present observations of another example of the signatures of coronal jets propagating into the outer corona and inner heliosphere. Our example differs from those of Yu et al. (2014, 2016) and Moore et al. (2015), in that their examples originate from polar coronal hole jets, while our examples here originate from coronal jets at equatorial latitudes and from the periphery of an AR. Our coronal jets are the same as those of Sterling et al. (2016), and that paper showed the jets connecting to white-light jets in the STEREO/COR1 FOV. Here we show that some of the coronal-jet signatures can be tracked to locations farther from the Sun.

### 4.1. Coronal-jet Origins

We give a brief summary of the solar origins of the coronal jets, more details of which are provided in Sterling et al. (2016). That paper studied a series of coronal jets that occurred at the edge of NOAA AR 11513. While they primarily used SDO/AIA data for their analysis, they also used complementary views from STEREO-B and showed that many of their

**Table 1**
Jets in the AIA 304 Å Animation

| Event | Prev. Event[a] | Start[b] | End[c] | Duration (minutes)[d] | Velocity (km $s^{-1}$)[e] | Rotations (Time Period)[f] | COR1 Velocity (km $s^{-1}$)[g] |
|---|---|---|---|---|---|---|---|
| J1 | ⋯ | 19:07:20 | ⋯ | ⋯ | 150 | 0.75 (19:14:32–19:19:20) | ⋯ |
| J2 | ⋯ | 19:19:56 | ⋯ | ⋯ | 190 | 0.50 (19:24:44–19:29:32) | ⋯ |
| J3 | 5 | 19:30:08 | 19:40:20 | 10 | 255 | 0(?)[h] | 368 ± 44 |
| J4 | 6 | 20:08:32 | 20:34:32 | 26 | 255 | 0.75 (20:14:32–20:24:08) | 479 ± 17 |
| J5 | 7(?)[i] | 20:37:20 | 21:09:08 | 32 | 170 | 1.5 (20:50:32–20:54:44) | 521 ± 32 |
| J6 | 8 | 21:17:32 | 21:49:20 | 32 | 615 | 0.25 (21:23:32–21:30:44) | 841 ± 10 |
| J7 | ⋯ | 22:57:08 | 23:24:44 | 28 | 270 | 0.5 (23:00:08–23:12:44 | ⋯ |
| J8 | ⋯ | 23:24:44 | 23:43:20 | 19 | 135 | 1.5 (23:25:56–23:28:56) | ⋯ |
| Averages | ⋯ | ⋯ | ⋯ | 24.5 ± 8.6 | 255 ± 155 | 0.8 ± 0.5 | |

**Notes.**
[a] Corresponding event number in Sterling et al. (2016), when determinable.
[b] Time of earliest clear brightening at the base of the erupting minifilament that makes the jet.
[c] Approximate time that base activity ceases for this event. Cannot be determined in some cases due to overlap with subsequent activity.
[d] Difference of previous two columns.
[e] Measured in 304 Å images over Figure 3 FOV, based on movement of bright spire features during the fast-rise phase (i.e., following an initial slow start to the minifilament's rise.
[f] Estimated number of $2\pi$ turns of the spire over time period given in parentheses.
[g] White-light jet velocity in STEREO-B/COR1 coronagraph images, as measured in Sterling et al. (2016).
[h] Spinning motion not obvious, but hard to determine with certainty that it does not exist.
[i] The brightening accompanying event 7 in Table 1 of Sterling et al. (2016) was from a location west of the Figure 4 FOV, but our 304 Å jet in the FOV of Figure 4 likely corresponds to the feature listed as jet 7 in the Sterling et al. (2016) COR1 animation.

coronal jets produced white-light jets in the STEREO-B COR1 FOV. While the AIA images showed that the COR1 features originated from several locations around the AR, here we concentrate on the features that made white-light jets in COR1 at a position angle of ≈315°; this is because it is at about this same position angle where we can identify white-light jets farther out in the corona. From the COR1 coronagraph animation of Sterling et al. (2016, the animation accompanying Figure 5 in that paper), it can be seen that the white-light jets from this position angle largely originated from location of the AR labeled "C" in that paper (see Figure 3(a) of Sterling et al. 2016). Hence we concentrate on coronal jets from that location in the following.

Figures 4(a)–(c), and the accompanying animation, show coronal jets from this location in AIA 304 Å, and Figures 4(d)–(f) and the accompanying animation, show the magnetic evolution of the region in SDO/HMI magnetograms. Table 1 lists the primary jets occurring from this location over 19:00–23:50 UT on 2012 June 30, which is the time period we will focus on. Figures 4(a)–(c) track the progress of jet J5 of Table 1.

As discussed in Sterling et al. (2016), the coronal jets from this location originate from either of the two neutral lines pointed to by the yellow and red arrows in Figure 4(d). Over the time of Figures 4(d)–(f), the positive-polarity patch between these arrows decreases in size; from the animation, this decrease is consistent with convergence of the positive-polarity flux patch and surrounding negative-polarity flux, resulting in flux cancellation. From this observation, in conjunction with our understanding of coronal-jet initiation outlined in Section 1, we conclude that it is likely that flux cancellation built a minifilament field that erupted to make the coronal jets, following the picture of Figure 1. The continued cancellation is responsible for the continuing series of essentially homologous coronal jets (Panesar et al. 2016a; Sterling et al. 2017).

In their study of 14 polar coronal hole jets, Moore et al. (2015) found that coronal jets that extended into white-light jets in the LASCO/C2 FOV tended to be those with relatively high amounts of twist when observed in AIA 304 Å images. Those jets reaching C2 had between 0.5 and 2.5 axial turns, with a peak near 1.5 turns. In contrast, they found that a more general population of 29 jets had axial rotations mostly between zero and 0.5 turns. Thus the jets that reach C2 preferentially have more twist than the general population of coronal hole jets.

Our coronal jets here are from an AR rather than a coronal hole, but we can ask whether these jets show spinning motions. Inspection of the 304 Å animation shows that several jets indeed appear to spin during their onset phase. We estimate the number of turns that each jet makes using the same basic procedure as in Moore et al. (2015), specifically by picking a feature on the jet, tracking its lateral motion, and counting how many apparent oscillations it makes in the left–right (east–west) direction during the early part of the jet. The black arrows in Figures 4(a)–(c) show an example where we track an absorbing feature in jet J5 of Table 1. Table 1 provides our results, giving our estimated number of turns for each jet. Other than jet J3, all of the jets show obvious indications of spin, where the values range from 0.25 to 1.5 turns, with an average of 0.8 turns. Only two of the eight jets (J3 and J6) have spin values smaller than the 0.5 lowest value of the Moore et al. (2015) coronal jets that made white-light jets.

Even though our interpretation of coronal-jet spin is based on visual inspection only, there is strong evidence from spectral studies providing evidence from Doppler measurements that many jets truly spin (e.g., Pike & Mason 1998; Kamio et al. 2010). Similar to the situation in Moore et al. (2015), the appearance is that the spinning is an *unwinding* of the field containing the cool 304 Å jet material, as the spinning eventually slows and stops in all of the cases.

We measured the outflow velocities of the coronal jets over the FOV of Figure 4, by tracking portions of the jet spire in emission in 304 Å; the absorbing material (likely erupting-minifilament material) sometimes moves out at a slower velocity. Jet J6 has a velocity higher than the others; this is

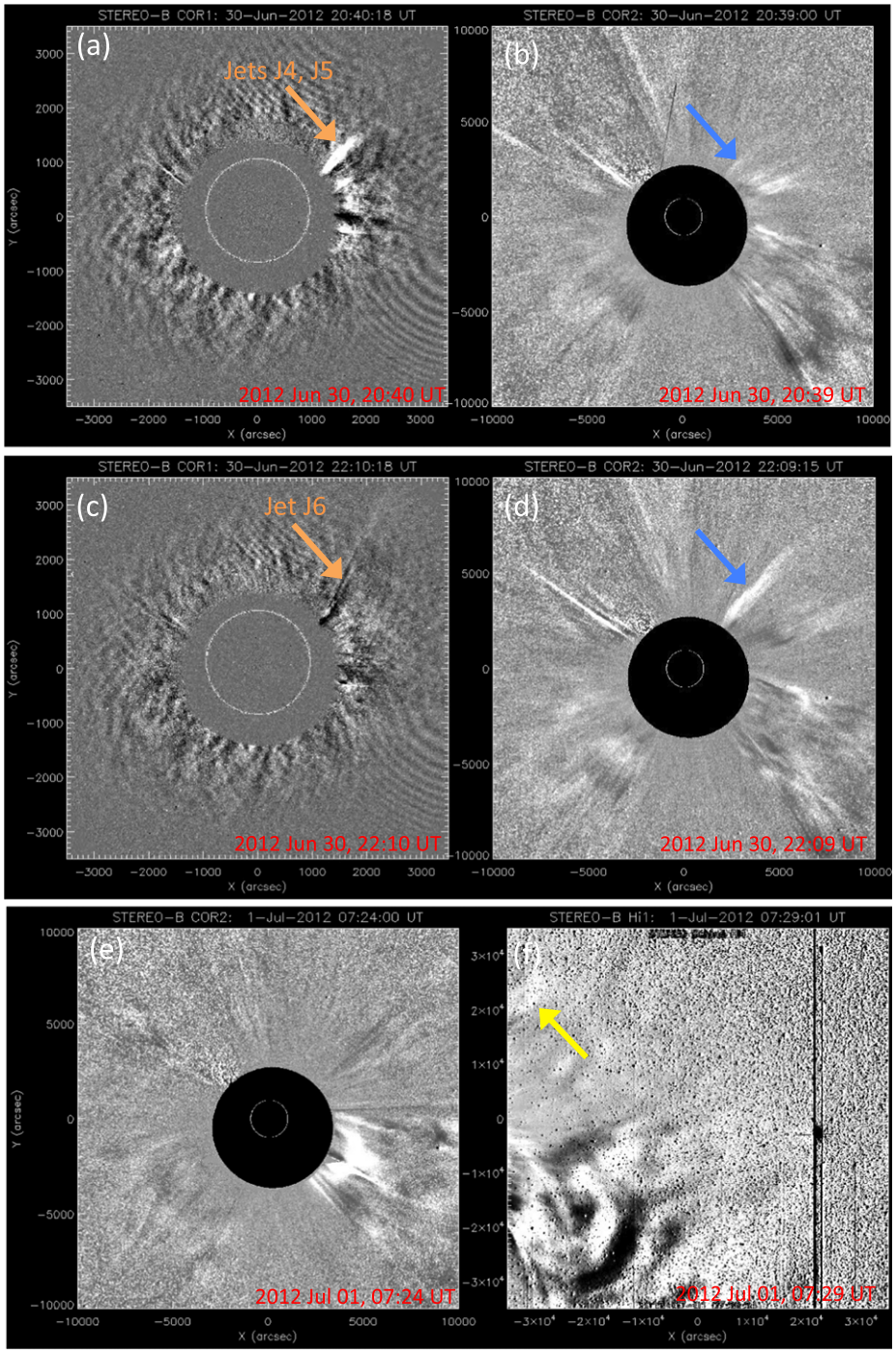


**Figure 5.** Outer-coronal and inner-heliospheric manifestations of coronal jets from AR 11513. These are coronagraph images from STEREO-B COR1 (a), (c) and COR2 (b), (d), (e), and a STEREO-B Hi1 heliospheric imager image (f). Horizontal pairs of images (a)–(b), (c)–(d), and (e)–(f), are, respectively, at approximately the same times. Sterling et al. (2016) identified the white-light jet in (a) as being due to coronal jets J4 and J5 of Table 1 (jets 6 and 7 of Sterling et al. 2016), and the white-light in (c) as due to coronal jet J6 of Table 1 (jet 8 of Sterling et al. 2016). Panels (b) and (d) show that these white-light jets remain intact (blue arrows) in the COR2 FOV (2.5–15 $R_{\odot}$), and (f) shows that the white-light jet in (d) persists into the Hi1 FOV (15–84 $R_{\odot}$ (yellow arrow). (That jet left the COR2 animation's FOV at about 2:09 UT, and hence is no longer visible in (e).) Thus it is plausible that the consequences of coronal jets depicted in Figure 4 can reach PSP locations, and be detected as switchbacks. An animation of this figure is available with the top portion showing the time evolution of the COR1 and COR2 images (panels (a)–(d)), at the 15 minute cadence of the available COR2 images (see Sterling et al. 2016 for a higher-cadence COR1 animation). The animation begins on 2012 June 30 at approximately 17:24 UT and ends at 2012 July 1 at approximately 02:55 UT. The realtime duration is 4 s. The bottom portion of the animation shows the time evolution of the COR2 and Hi1 images (panels (e)–(f)), at the 40 minute cadence of the available Hi1 images. This part of the animation begins on 2012 June 30 at around 16:49 UT and ends on 2012 July 1 at about 23:29 UT. Its realtime duration is 5 s.

(An animation of this figure is available.)

probably due to a stronger energy release, as it corresponds to an explosive flare of GOES level C1.6. Sterling et al. (2016) also found that this coronal jet extended to a COR1 white-light jet that was the fastest of their set: 841 km $s^{-1}$. This is consistent with the study of Shen et al. (2011a), which provides observational evidence that the GOES class of a flare is directly

related to the kinetic energy of the accompanying erupting filament.

### 4.2. The Jets in the Outer Corona

Figure 5(a) shows the progression of the jets J4 and J5 into the STEREO/COR1 coronagraph FOV, based on the results of Sterling et al. (2016, see Figure 5 and the accompanying animation of that paper; in that paper, our jets J4 and J5 are, respectively, jets 6 and 7). Figure 5(b) shows the jets in the STEREO-B COR2 coronagraph, and the accompanying animation shows that this feature is clearly a continuation of the jet J4/J5 feature of Figure 5(a). From the 5 minute cadence COR1 animation in Sterling et al. (2016), these two jets occur very closely together in time in COR1, and so we cannot differentiate between them in the 15 minute cadence COR2 animation (in the animation of Figure 5 the cadence of both the COR1 and COR2 animations are set to match the cadence of the COR2 animations). Figure 5(c) shows jet J6 of Table 1 (this identification between J6 and the COR1 jet was made in Sterling et al. (2016) using the 5 minute cadence COR1 animation). Figure 5(d) shows a white-light jet in COR2 from the same time and position angle; this is either a continuation of jet J4/J5, or it could be jet J6, or a combination of jets, but the time cadence of COR2 is not high enough for us to determine which of these is the case. In the COR2 animation, the white-light jet of Figures 5(b) and (d) has velocity of about 800 km $s^{-1}$.

### 4.3. The Jets in the Inner Heliosphere

Figure 5 shows a COR2 image in Figure 5(e), concurrent with a STEREO-B Hi1 image in Figure 5(f). Hi1 observes the inner heliosphere with a wide FOV (15–84 $R_{\odot}$; Howard et al. 2008), but offset from Sun center; in Figure 5(f) the Sun is located off of the left side of the panel. From the accompanying animation the jet in Figure 5(f) is a continuation of one of, or a combination of some of, the Table 1 jets that have already left the FOV of Figure 5(e). We can confirm that the location of the jet with the arrow in Figure 5(f) corresponds to the position angle of the Table 1 jets by using the large-scale eruption that appears in COR2 at 12:09 UT in the animation. That eruption is very large, and expands out into a CME that is visible in the Hi1 animation from 15:29 UT. This feature is an unmistakable continuation of the COR2 eruption. In the Hi1 animation, it has a position angle slightly smaller than (just clockwise of) that of the Table 1 jets, and this gives us confidence that the jet seen in Hi1 at a slightly larger position angle in Figure 5(f) indeed corresponds to the jets of Table 1. (The large eruption beginning at 12:09 UT in COR2 originates from a neutral line to the east of the images in Figure 4; in Sterling et al. 2016, the source location is between locations marked "A" and "B" in Figure 3(a) of that paper.) That large eruption was of a larger scale than those that make the jets at location displayed in Figure 4. In the Hi1 FOV, the white-light jet of Figure 5(f) has a velocity of about 750 km $s^{-1}$; to within the uncertainties of our estimate, this can be regarded as about the same as the velocity of the white-light jet (or combination of jets) observed in COR2 (Section 4.2).

## 5. Discussion

Because coronal jets are frequent, and because recent work suggests that they are formed when magnetic flux ropes erupt away from the solar surface and reconnect with coronal field (Figure 1), it is natural to ask whether the coronal jets could be the source of the magnetic switchback fluctuations observed by PSP in the near-Sun solar wind. We have presented a picture (Figures 2 and 3) by which the Alfvénic fluctuations resulting from the magnetic eruptions that produce the jets might evolve into switchbacks. We have also presented evidence that jets at equatorial latitudes can reach the outer corona and the inner heliosphere (Figure 5), supplementing earlier studies of white-light jets and solar-wind disturbances from coronal jets from polar regions (Section 4). Moreover, numerical simulations support that disturbances put onto an open field in the corona can persist out to many solar radii (Tenerani et al. 2020).

Our idea presented in Figure 3 addresses how the Alfvénic fluctuations from coronal jets might lead to Alfvénic-pulse packets on magnetic fields. Furthermore, our picture provides an explanation for why the pulse field's angle of inclination to the radial field would increase with radial distance from the Sun, a tendency which has been observed (Mozer et al. 2020). It is, however, not clear to us how the angle could be increased to an angle of much more than 90°, such that the field literally "switches back" on itself (e.g., as in extended data Figure 2 of Kasper et al. 2019). It seems, however, that only a small percentage of switchbacks have such rotation angles far beyond 90° (Mozer et al. 2020). Perhaps a nonlinear and/or turbulent effect, or some additional process in the solar wind, could augment the progression pictured in Figure 3(c), so that the field's angle greatly exceeds 90° in some cases.

Our suggested connection between coronal jets and switchbacks is, however, still speculation, and therefore other ideas cannot be ruled out (e.g., Tenerani et al. 2020). Mapping a switchback, perhaps a particularly large one, back along a Parker spiral to a magnetic footpoint on which a jet or series of jets is observed with the proper timing would provide support for this idea. In addition, we hope that simulations of coronal jets that include the magnetic connections between the solar surface and the heliosphere (e.g., Lionello et al. 2016; Roberts et al. 2018), with the addition of driving the event by a minifilament-field eruption, will be able to test these ideas.

We thank an anonymous referee for helpful comments. This work was supported by funding from the Heliophysics Division of NASA's Science Mission Directorate through the Heliophysics Guest Investigators (HGI) Program, and the MSFC Hinode Project.

## ORCID iDs

Alphonse C. Sterling https://orcid.org/0000-0003-1281-897X

## References

Alzate, N., & Morgan, H. 2016, ApJ, 823, 129
Bale, S. D., Badman, S. T., Bonnell, J. W., et al. 2019, Natur, 576, 237
Bale, S. D., Goetz, K., Harvey, P. R., et al. 2016, SSRv, 204, 49
Bemporad, A., Sterling, A. C., Moore, R. L., & Poletto, G. 2005, ApJ, 635L, 189
Chen, H., Zhang, J., & Ma, S. 2012, RAA, 12, 573
Cirtain, J. W., Golub, L., Lundquist, L., et al. 2007, Sci, 318, 1580
Duan, Y., Shen, Y., Chen, H., & Liang, H. 2019, ApJ, 881, 132
Dudok de Wit, T., Krasnoselskikh, V. V., Bale, S. D., et al. 2020, ApJS, 246, 39
Fox, N. J., Velli, M. C., Bale, S. D., et al. 2016, SSRv, 204, 7
Hinode Review Team, Khalid, A.-J., Patrick, A., et al. 2019, PASJ, 71, R1

Hong, J., Jiang, Y., Yang, J., et al. 2013, RAA, 13, 253
Hong, J., Jiang, Y., Yang, J., et al. 2014, ApJ, 796, 73
Horbury, T. S., Woolley, T., Laker, R., et al. 2020, ApJS, 246, 45
Howard, R. A., Moses, J. D., Vourlidas, A., et al. 2008, SSRv, 136, 67
Kahler, S. W., Crooker, N. U., & Gosling, J. T. 1996, JGR, 101, 24373
Kamio, S., Curdt, W., Teriaca, L., Inhester, B., & Solanki, S. K. 2010, A&A, 510, 1
Kasper, J. C., Abiad, R., Austin, G., et al. 2016, SSRv, 204, 131
Kasper, J. C., Bale, S. D., Belcher, J. W., et al. 2019, Natur, 576, 228
Kumar, P., Karpen, J. T., Antiochos, S. K., et al. 2018, ApJ, 873, 93
Lionello, R., Török, T., Titov, V. S., et al. 2016, ApJL, 831, L2
Liu, J., Wang, Y., & Erdélyi, R. 2019, FrASS, 6, 44L
McGlasson, R. A., Panesar, N. K., Sterling, A. C., & Moore, R. L. 2019, ApJ, 882, 16
Miao, Y., Liu, Y., Li, H. B., et al. 2018, ApJ, 869, 39
Moore, R. L., Cirtain, J. W., Sterling, A. C., & Falconer, D. A. 2010, ApJ, 720, 757
Moore, R. L., Sterling, A. C., Falconer, D. A., & Robe, D. 2013, ApJ, 769, 134
Moore, R. L., Sterling, R. L., & Falconer, D. A. 2015, ApJ, 806, 11
Moore, R. L., Sterling, R. L., & Panesar, N. K. 2018, ApJ, 859, 3
Mozer, F. S., Agapitov, O. V., Bale, S. D., et al. 2020, ApJS, 246, 68
Nisticò, G., Bothmer, V., Patsourakos, S., & Zimbardo, G. 2009, SoPh, 259, 87
Nisticò, G., Bothmer, V., Patsourakos, S., & Zimbardo, G. 2010, AnGeo, 28, 687
Panesar, N. K., Sterling, A. C., & Moore, R. L. 2016a, ApJ, 822L, 7
Panesar, N. K., Sterling, A. C., & Moore, R. L. 2017, ApJ, 844, 131
Panesar, N. K., Sterling, A. C., & Moore, R. L. 2018a, ApJ, 853, 189
Panesar, N. K., Sterling, A. C., Moore, R. L., et al. 2018b, ApJ, 868L, 27
Panesar, N. K., Sterling, A. C., Moore, R. L., & Chakrapani, P. 2016b, ApJ, 832L, 7
Paraschiv, A. R., Lacatus, D. A., Badescu, T., et al. 2010, SoPh, 264, 365
Pike, C. D., & Mason, H. E. 1998, SoPh, 182, 333
Raouafi, N. E., Patsourakos, S., Pariat, E., et al. 2016, SSRv, 201, 1
Raouafi, N. E., & Stenborg, G. 2014, ApJ, 787, 118
Roberts, M. A., Uritsky, V. M., DeVore, C R., & Karpen, J. T. 2018, ApJ, 866, 14
Savcheva, A., Cirtain, J., Deluca, E. E., et al. 2007, PASJ, 59, 771
Shen, Y., Liu, Y., & Liu, R. 2011a, RAA, 11, 594
Shen, Y., Liu, Y., Su, J., & Deng, Y. 2012, ApJ, 745, 164
Shen, Y., Liu, Y., Su, J., & Ibrahim, A. 2011b, ApJ, 735L, 43
Shen, Y., Liu, Y. D., Su, J., Qu, Z., & Tian, Z. 2017, ApJ, 851, 67
Shen, Y., Qu, Z., Zhou, C., et al. 2019, ApJ, 855L, 11
Shibata, K., Ishido, Y., Acton, L. W., et al. 1992, PASJ, 44, L173
Shibata, K., & Magara, T. 2011, LRSP, 8, 6
Shibata, K., & Uchida, Y. 1986, SoPh, 178, 379
Solanki, R., Srivastava, A. K., Rao, Y. K., & Dwivedi, B. N. 2019, SoPh, 294, 68
Sterling, A. C., Moore, R. L., Falconer, D. A., et al. 2016, ApJ, 821, 100
Sterling, A. C., Moore, R. L., Falconer, D. A., & Adams, M. 2015, Natur, 523, 437
Sterling, A. C., Moore, R. L., Falconer, D. A., Panesar, N. K., & Martinez, F. 2017, ApJ, 844, 28
Sterling, A. C., Moore, R. L., & Panesar, N. K. 2018, ApJ, 864, 68
Suess, S. 2007, in ESA SP-641, Proc. Second Solar Orbiter Workshop, ed. E. Marsch, L. Tsinganos, R. Marsden, & L. Conroy (Noordwijk: ESA), 11
Tenerani, A., Velli, M., Matteini, L., et al. 2020, ApJS, 246, 32
Wang, Y.-M., Sheeley, N. R., Jr, Socker, D. G., et al. 1998, ApJ, 508, 899
Wyper, P. F., Antiochos, S. K., & DeVore, C. R. 2017, Natur, 544, 452
Wyper, P. F., DeVore, C. R., & Antiochos, S. K. 2018, ApJ, 852, 98
Yamauchi, Y., Suess, S. T., Steinberg, J. T., & Sakurai, T. 2004, JGRA, 109, A03104
Yokoyama, T., & Shibata, K. 1995, Natur, 375, 42
Young, P. R., & Muglach, K. 2014a, SoPh, 289, 3313
Young, P. R., & Muglach, K. 2014b, PASJ, 66, 12
Yu, H.-S., Jackson, B. V., Buffington, A., et al. 2014, ApJ, 784, 166
Yu, H.-S., Jackson, B. V., Yang, Y. H., et al. 2016, JGRA, 121, 4985